



RESEARCH ARTICLE

10.1029/2020JA028786

Flux Transfer Events at a Reconnection-Suppressed Magnetopause: Cassini Observations at Saturn

Key Points:

- Eight Saturn ion-scale flux transfer events (FTEs) are analyzed with diameters of $d_i \sim 1-27$
- FTEs at Saturn are found to transfer negligible amounts of flux at Saturn's magnetosphere
- Evidence for electron energization is observed inside some of the FTEs, due to either Fermi acceleration or parallel electric fields

Jamie M. Jasinski¹ , Mojtaba Akhavan-Tafti² , Weijie Sun² , James A. Slavin² , Andrew J. Coates^{3,4} , Stephen A. Fuselier^{5,6} , Nick Sergis⁷ , and Neil Murphy¹

¹NASA Jet Propulsion Laboratory, California Institute of Technology, Pasadena, CA, USA, ²Department of Climate and Space Sciences and Engineering, University of Michigan, MI, USA, ³Mullard Space Science Laboratory, UCL, Dorking, UK, ⁴Center for Planetary Sciences at UCL/Birkbeck, London, UK, ⁵Southwest Research Institute, San Antonio, TX, USA, ⁶Department of Physics and Astronomy, University of Texas at San Antonio, San Antonio, TX, USA, ⁷Office for Space Research, Academy of Athens, Athens, Greece

Correspondence to:

J. M. Jasinski,
jasinski@jpl.nasa.gov

Citation:

Jasinski, J. M., Akhavan-Tafti, M., Sun, W., Slavin, J. A., Coates, A. J., Fuselier, S. A., et al. (2021). Flux Transfer Events at a reconnection-suppressed magnetopause: Cassini observations at Saturn. *Journal of Geophysical Research: Space Physics*, 126, e2020JA028786. <https://doi.org/10.1029/2020JA028786>

Received 4 OCT 2020
Accepted 25 DEC 2020

Abstract We present the discovery of seven new flux transfer events (FTEs) at Saturn's dayside magnetopause by the Cassini spacecraft and analyze the observations of all eight known FTEs. We investigate how FTEs may differ at Saturn where the magnetopause conditions are likely to diamagnetically suppress magnetic reconnection from occurring. The measured ion-scale FTEs have diameters close to or above the ion inertial length $d_i \sim 1-27$ (median and mean values of 5 and 8), considerably lower than typical FTEs found at Earth. The FTEs magnetic flux contents are 4–461 kWb (median and mean values of 16 and 77 kWb), considerably smaller (<0.1%) than average flux opened during magnetopause compression events at Saturn. This is in contrast to Earth and Mercury where FTEs contribute significantly to magnetospheric flux transfer. FTEs therefore represent a negligible proportion of the amount of open magnetic flux transferred at Saturn. Due to the likely suppression of the two main growth-mechanisms for FTEs (continuous multiple x-line reconnection and FTE coalescence), we conclude that adiabatic expansion is the likely (if any) candidate to grow the size of FTEs at Saturn. Electron energization is observed inside the FTEs, due to either Fermi acceleration or parallel electric fields. Due to diamagnetic suppression of reconnection at Saturn's magnetopause, we suggest that the typical size of FTEs at Saturn is most likely very small, and that there may be more $d_i \sim 1$ FTEs present in the Cassini magnetometer data that have not been identified due to their brief and unremarkable magnetic signatures.

1. Introduction

Magnetic reconnection is a phenomenon that rearranges the topology of magnetic fields resulting in magnetic energy being transferred to particles. It is therefore a primary mechanism for energizing space plasmas (see recent book Gonzalez & Parker, 2016). Magnetic reconnection occurs at various locations in the solar system, for example, in the solar chromosphere during solar flares, and in the solar wind and inside coronal mass ejections (e.g. Gosling, 2012; Liewer et al., 2013). Magnetic reconnection also occurs at the magnetopause boundary at planetary magnetospheres and has important effects on the structure and dynamics of the terrestrial magnetosphere (Dungey, 1961). Flux transfer events (FTEs) are transient magnetic structures that are a result of reconnection occurring at the dayside magnetopause of a magnetosphere (e.g. Fear et al., 2008). FTEs are twisted helical flux tubes which are often called flux ropes, and were first observed at the Earth's magnetopause (Rijnbeek, 1984; Russell & Elphic, 1978, 1989). The FTE flux rope structure is shown in Figure 1a, with a core field directed orthogonally to the outer layers of magnetic flux. The mechanism that generates FTEs at the magnetopause is generally accepted to be simultaneous multiple x-line reconnection (e.g. Lee & Fu, 1985; 1986).

FTEs are commonly observed at the inner planet magnetospheres of Earth and Mercury. At Mercury, FTEs are so common and are generated at such high rates at the dayside magnetopause that their observation during a typical magnetopause crossing by a spacecraft have earned the name of "FTE showers" (Slavin et al., 2012; Sun, Slavin, Smith et al., 2020). FTEs are also commonly observed and well-studied at Earth's magnetopause by a variety of spacecraft as well as in numerical simulations (e.g. Akhavan-Tafti et al., 2020; Eastwood et al., 2016; Lockwood & Hapgood, 1998; Varsani et al., 2014). However, the conditions at a

© 2021. The Authors.
This is an open access article under the terms of the Creative Commons Attribution License, which permits use, distribution and reproduction in any medium, provided the original work is properly cited.

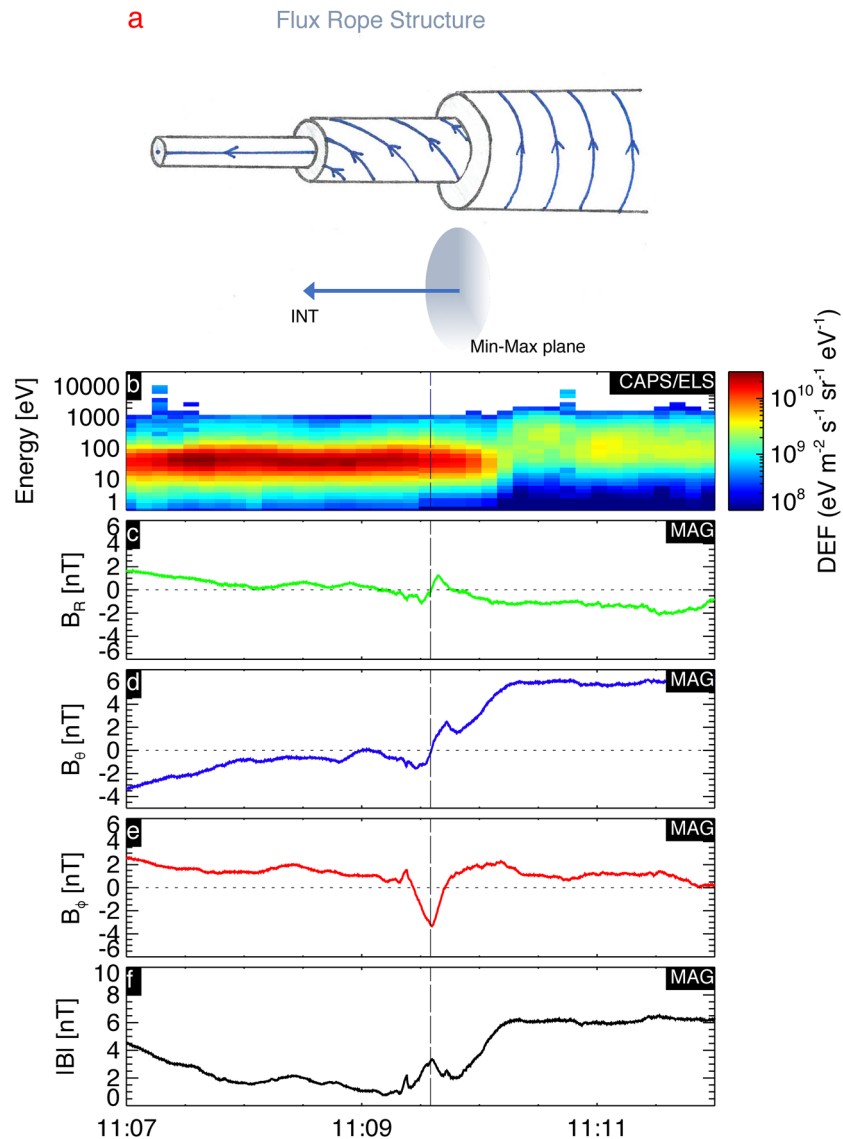


Figure 1. Flux transfer event structure and observations. Panel (a) shows the helical structure of a cylindrical force-free flux rope, with a core field in the axial direction (labeled “INT”) and the outer layer orientated perpendicular to the core. Panels (b)–(d) show observations of an FTE crossing at Saturn’s magnetopause by the Cassini spacecraft on February 4, 2007. Panel (b) shows the electron differential energy flux (DEF) measured by CAPS-ELS, with the background and photoelectron flux removed; (c)–(e) show the three components of the magnetic field in KRTP coordinates measured by MAG; and (f) shows the resulting magnetic field magnitude. The schematic shown in (a) is taken from Jasinski, Slavin et al. (2016).

magnetopause vary at different planetary magnetospheres. As the solar wind expands radially outwards throughout the solar system, the solar wind magnetosonic Mach number increases with radial distance from the Sun, resulting in higher plasma- β magnetosheaths at the outer planet magnetospheres (where plasma- β is the plasma to magnetic field pressure ratio). This leads to a large difference in plasma- β across the magnetopause, which acts to suppress magnetic reconnection from occurring unless the magnetic shear across the boundary is very high (e.g. Quest & Coroniti, 1981; Swisdak et al., 2003).

At the outer planets, such as at Saturn’s magnetopause this effect is most pronounced. A survey of Cassini magnetopause crossings at Saturn (Masters et al., 2012) found that the change in plasma- β across the magnetopause was significantly higher than at Earth, and that typical conditions would require significantly higher magnetic shears to be conducive to reconnection. The requirement for higher shear results in the

general assertion that reconnection at Saturn's magnetopause is usually suppressed from occurring (Masters, 2015). This suppression however does not mean that reconnection is absent at Saturn. Many studies have reported evidence of reconnection at Saturn's dayside magnetopause, such as: the discovery of the first FTE at Saturn (Jasinski, Slavin et al., 2016); magnetospheric electron beams present in the magnetosheath due to the occurrence of reconnection (Badman et al., 2013; Fuselier et al., 2014, 2020; Sawyer et al., 2019); magnetosheath plasma injected into Saturn's high-latitude cusps after low-latitude dayside magnetic reconnection (Arridge et al., 2016; Jasinski et al., 2014, 2017) and high-latitude lobe reconnection (Jasinski, Arridge et al., 2016) as well as a multitude of auroral observations of reconnection signatures (e.g. Badman et al., 2013; Kinrade et al., 2017; Palmaerts et al., 2016; Radioti et al., 2013).

There is, however, the existing question of the exact nature of FTE flux rope generation at a magnetopause such as Saturn's, where reconnection is typically suppressed from occurring. How important are FTEs in contributing to the flux circulation in Saturn's magnetosphere? How (and can) FTEs grow to large scales such as those observed at Earth, with diameters equal up to $\sim 500 d_i$ (ion inertial lengths)? In this paper we attempt to understand FTEs and FTE generation at Saturn's magnetopause, by presenting the discovery of seven new FTEs at Saturn's magnetopause, and analyzing all eight known FTEs (including the first and only previously reported FTE observation reported by Jasinski, Slavin et al., 2016). We present the Observations and Analysis in the following section, and then discuss the results in Section 3.

2. Observations and Analysis

We label the FTEs by the date they were observed in the "dd-mmm-yyyy" format. If multiple FTEs were observed on the same day, we provide a letter suffix listed alphabetically (i.e. a, b).

2.1. Instrumentation

In this paper, we use the following Cassini instrumentation: the Magnetometer (MAG; Dougherty et al., 2004); Cassini Plasma Spectrometer (CAPS; Young et al., 2004) and the Low-Energy Magnetospheric Measurement System (LEMMS; Krimigis et al., 2004). MAG data is presented in a spherical polar coordinate Kronographic-Radial-Theta-Phi (KRTP) system. R is directed in the planet-spacecraft direction, ϕ is in the direction of Saturn's rotation, and θ completes the right-hand set and is directed in the colatitudinal direction and is positive southwards. For readers more familiar with a magnetospheric cartesian system, θ is approximately in the $-Z$ direction, while R and ϕ are dependent on the location of Cassini with respect to Saturn and the Sun. At the subsolar region this would correspond to $R \sim -X$ and $\phi \sim Y$, while at dawn local time $R \sim Y$ and $\phi \sim X$. KRTP is useful when studying the dayside magnetopause as the vector direction normal to the magnetopause is in the $\sim -R$ direction, ϕ is approximately pointing duskward along the dayside magnetopause and θ lies along the projection of the dipole axis onto the magnetopause and is positive southwards.

The CAPS instrument consists of the Electron Spectrometer (ELS) and the Ion Mass Spectrometer (IMS). ELS is a hemispherical top-hat electrostatic analyzer that measures electron flux as a function of energy-per-charge with an energy range of 0.58–28,250 eV/e. The electrons pass into the instrument and strike a microchannel plate which causes a secondary electron cascade that are then collected by eight anodes. The eight anodes field-of-view (FOV) point in different directions, which means the instrument can therefore sample different pitch angles. The instrument is also mounted on an actuating platform to increase the FOV. For more details on the ELS instrument we direct the reader to the methods section (i.e. Section 2) of Jasinski et al. (2019) and references therein. IMS is also a hemispherical top-hat electrostatic analyzer, also with eight anodes. IMS measures the ion flux with an energy-per-charge range of 1–50,280 eV/e. IMS also uses a time-of-flight analyzer to measure the mass-per-charge of the ions, and can therefore determine the ion composition. We refer the reader to Thomsen et al. (2010) and Felici et al. (2018) for more information about IMS and processing of its data. We also present electron measurements from the LEMMS instrument, in an energy range of 15 keV–0.88 MeV (i.e. a higher energy range than ELS), which is part of the Magnetospheric Imaging Instrument (MIMI).

Table 1

List of FTEs Date, Time and Location with Respect to Saturn, Including the First FTE Discovered (Denoted in the Table by *) at Saturn Which was Reported by Jasinski, Slavin et al. (2016)

Date	FTE time (UT)	R (R _S)	Latitude (°)	Local time (hh:mm)
09-Oct-2005 (a)	17:28:41–17:28:58	23.9	−0.3	08:58
09-Oct-2005 (b)	17:32:32–17:32:35	"	"	"
10-Oct-2005	06:06:53–06:07:05	20.5	−0.3	09:19
02-Feb-2007 (a)	11:28:31–11:28:54	16.4	−37.7	12:05
02-Feb-2007 (b) *	23:33:55–23:34:21	17.3	−24.0	12:50
04-Feb-2007	11:09:26–11:09:40	20.6	8.2	14:14
02-May-2008	15:44:16–15:44:22	18.8	−3.0	10:55
30-Aug-2008	10:17:01–10:17:21	20.3	9.9	10:50

Multiple FTEs observed in one day are assigned a letter suffix (i.e. ‘a’ and ‘b’) and are referred to as such in the article).

2.2. Example of an FTE-type Flux Rope Observation at Saturn

Observations from the crossing of an FTE on February 4th 2007 (i.e. 04-Feb-2007) are shown in Figures 1b–1f as an example of a newly discovered FTE in the Cassini magnetometer data. Figure 1b shows electron measurements made by CAPS-ELS. The background flux and photoelectrons have been removed, and data from all eight anodes have used to estimate an omnidirectional flux. This has been completed using the method developed by Arridge et al. (2009) and also used and described by Jasinski et al. (2019).

The CAPS-ELS measurements show that Cassini was in the magnetosheath at the start of the timeseries, as observed by the high fluxes of electrons observed at energies of <100 eV. The magnetopause current layer (MPCL) is centered at ~11:10 UT, and the dashed line just before shows the center of the FTE crossing. Upon crossing the MPCL, Cassini enters the magnetosphere where more energetic electrons (i.e. 10–1,000 eV) are measured with lower fluxes. Figures 1c–1f show the magnetometer measurements. In the magnetosheath the magnetic field is lower (2–4 nT) than in the magnetosphere (~6 nT). The magnetic field upon entering the magnetosphere rotates to be directed in the magne-

tospheric direction (i.e. B_{θ}). During the FTE crossing we observe the magnetic field rotate and peak in B_{ϕ} , corresponding to the measurement of the core field of the FTE (in the schematic of Figure 1a this would be the core field labeled as “INT”); as well as bipolar signatures in B_R and B_{θ} . This is a typical observation of an FTE, with signature characteristics such as a peak in the core field as well as a bipolar transition in the R and θ components.

In addition to the new FTE shown in Figure 1, we have also discovered six other new FTEs. All seven new FTEs are listed in Table 1, along with their times and location with respect to Saturn. We also list the FTE reported by Jasinski, Slavin et al. (2016), marked by an asterisk, and this FTE is also included in all the analysis shown in this paper.

2.3. Minimum Variance Analysis (MVA)

We use minimum variance analysis (MVA) to categorize and understand the magnetic signatures of the observed FTE flux ropes at Saturn’s magnetopause. First developed by Sonnerup and Cahill (1967) MVA transforms the magnetic field data into an orthogonal coordinate system where the unit vectors are aligned in the minimum, maximum and intermediate variance directions. The minimum variance direction represents the direction that the flux rope passed over the spacecraft, while the intermediate vector corresponds to the axis of the flux rope (e.g. Xiao et al., 2004). If the spacecraft crossed through the center of the flux rope then B_{\min} will be zero throughout the flux rope crossing. However, as the impact factor (“IP”—i.e. closest approach to the flux rope core) increases then B_{\min} will also increase. In a cylindrically shaped FTE as shown in the schematic in Figure 1a, a bipolar signature will be observed in B_{\max} , with a value of zero at closest approach to the flux rope core; this will also be where B_{int} will peak. MVA has been used with various magnetometer measurements to understand magnetic structure at planetary magnetospheres throughout the solar system (e.g., Eastwood et al., 2002; Jasinski, Slavin et al., 2016; Knetter et al., 2004; Slavin et al., 2014; Smith et al., 2017; Sonnerup & Scheible, 1998; Sun, Slavin, Dewey et al., 2020).

The magnetic field measurements of each FTE crossing in MVA coordinates are shown as a timeseries in Figure 2. All FTE crossings feature an obvious bipolar signature in B_{\max} , an increase in magnitude in the core (B_{INT}) direction at the midpoint of the FTE crossing, as well as a nonvarying B_{\min} field. The start-stop times of the FTEs were based on the method by Jasinski, Slavin et al. (2016) and were selected qualitatively by-eye to coincide with the peaks of the bipolar signature in B_{\max} , and contain the increase in core field as well as maintain a minimally varying B_{\min} . More detailed MVA results for the 04-Feb-2007 FTE observation can be seen in Figure 3. Figures 3a and 3b show hodograms of the magnetometer measurements in the minimum, intermediate and maximum vector directions, while a timeseries of these observations are shown

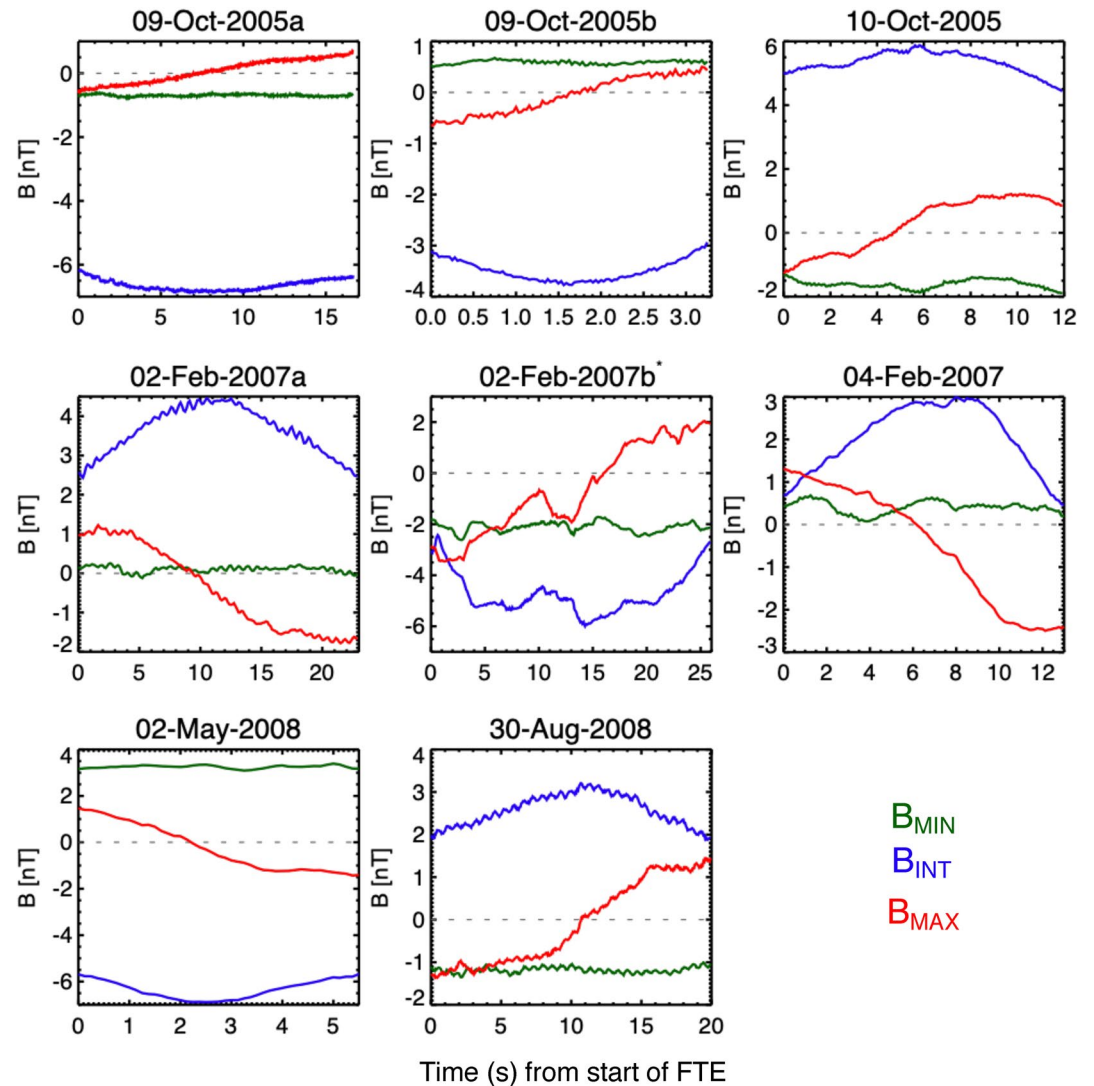


Figure 2. Magnetic field measurements of all the FTEs in MVA coordinates. The data is shown as a timeseries with the $t = 0$ s representing the start of the FTE crossing which are mentioned in Table 1.

in Figures 3c–3e in black. The hodograms and timeseries show that B_{MIN} was close to zero throughout the FTE, which shows that the spacecraft crossed through the FTE close to its center (i.e. the impact factor was close to zero). B_{MAX} shows a very discernible bipolar signature in both hodograms and timeseries, beginning at ~ 1.5 nT and ending at ~ -2.5 nT. B_{INT} peaks at ~ 3 nT and is orientated largely in the B_{ϕ} direction (see Table 2), which points azimuthally along the magnetopause, which is the generally the direction expected for multiple x-line generated FTEs as described by Lee and Fu (1987). A summary of the MVA results for all the FTEs are shown in Table 2.

2.4. Flux Rope Modeling

Magnetic signatures of the FTEs were compared to a force-free cylindrical flux rope model, first described by Lundquist (1950) and further developed by Lepping et al. (1990, 1995). In a force-free magnetic field the current density \mathbf{J} is parallel to the magnetic field (i.e. $\mathbf{J} \times \mathbf{B} = 0$), and therefore:

$$\nabla \times \mathbf{B} = \mu_0 \mathbf{J} = \alpha \mathbf{B} \quad (1)$$

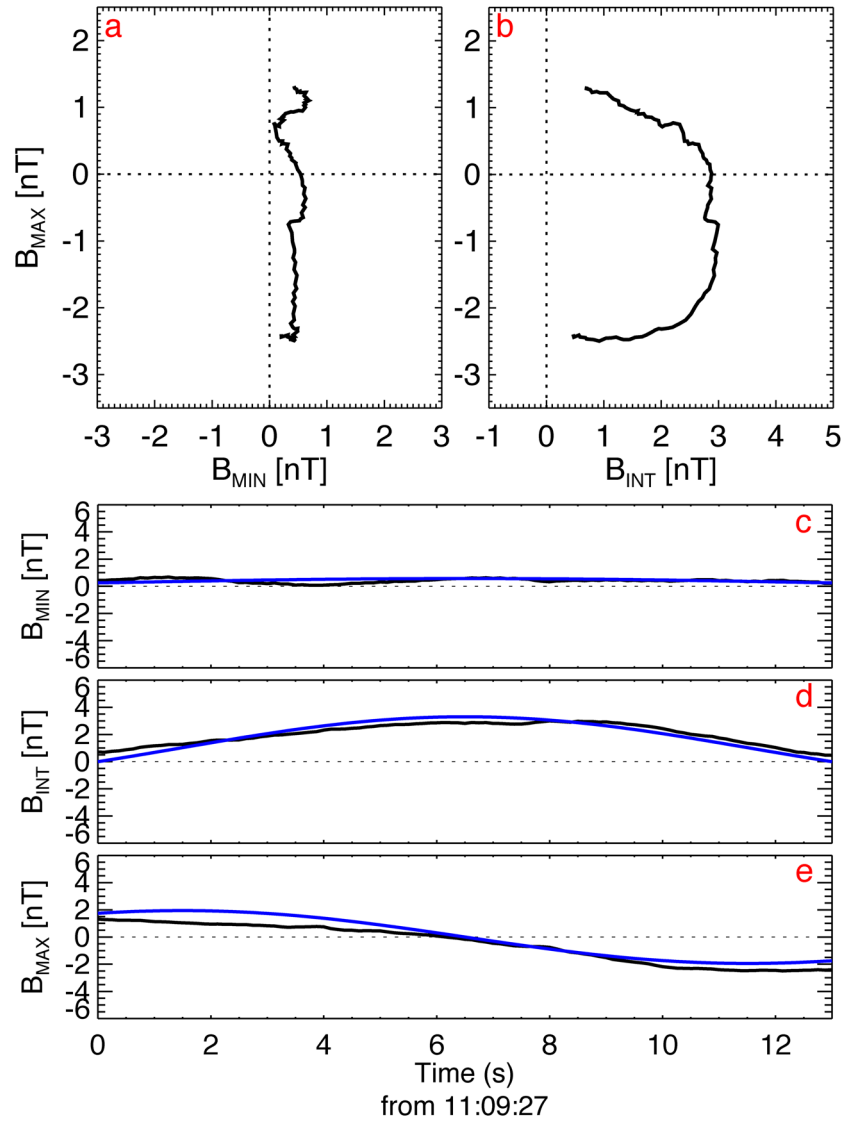


Figure 3. Flux Transfer Event analysis results using MVA and model fitting for the observation made for 04-Feb-2007 FTE. Panels (a) and (b) show hodograms of the magnetic field measurements in MVA coordinates; (c–f) show the same data in black as a timeseries, as well as the force-free model (blue). Table 3 contains a summary of MVA and model results.

Taking the curl of both sides of Equation 1:

$$\nabla^2 \mathbf{B} = -\alpha^2 \mathbf{B} \quad (2)$$

In cylindrical coordinates, the solution to Equation 2 is a Bessel function of the first kind:

$$B_A = B_0 J_0 \left(\frac{\alpha r}{R_{FR}} \right)$$

$$B_T = HB_0 J_1 \left(\frac{\alpha r}{R_{FR}} \right)$$

$$B_R = 0 \quad (3)$$

Table 2
FTE Flux Rope Parameter Estimates From MVA and Force-free modeling

FTE date	Core direction (R, θ, ϕ)	IP	B_0 (nT)	χ^2	Duration (s)	V_{TOT} (km/s)	FTE diameter (km)	FTE diameter (d_i)	Flux content (kWb)
09-Oct-2005 (a)	(0.25, -0.4, -0.88)	0.11	6.9	0.5	17	141	2,397	3.7	13
09-Oct-2005 (b)	(-0.74, 0.68, 0.04)	0.16	3.9	0.46	3	178	534	0.8	0.4
10-Oct-2005	(0.26, -0.40, -0.88)	0.27	6.5	0.39	12	195	2,340	4.7	12
02-Feb-2007 (a)	(0.97, 0.15, -0.20)	0.03	4.5	0.26	23	206	4,738	10.7	34
02-Feb-2007 (b) *	(-0.15, 0.31, -0.94)	0.34	6.9	0.16	26	540	14,040	27	461
04-Feb-2007	(-0.31, -0.25, -0.92)	0.14	3.4	0.05	14	114	1,596	2.5	3
02-May-2008	(-0.13, 0.25, -0.96)	0.43	8.8	0.35	6	165	990	1.5	3
30-Aug-2008	(-0.40, 0.91, 0.13)	0.35	3.7	0.17	20	100–300 ^a	2000–6000 ^a	5.5–16.6 ^a	20–180 ^a

Note. IP is the impact factor, which is a measure of how close the spacecraft was to the FTE core at its closest approach.

^aWe provide a range due to questionable velocity moment estimation.

where B_0 is the magnitude of the magnetic field at the center of the rope; r/R_{FR} is the normalized impact factor, J_0 and J_1 are the zeroth and first-order Bessel functions, and H is the helicity of the structure (equal to ± 1). α is a constant proportionality factor, set to 2.405, so that the magnetic field in the flux rope is in the axial direction (the intermediate direction) at the center of the flux rope and is tangential at the edge of the flux rope (i.e. the value at which J_0 is equal to zero is at 2.405, and therefore represents the edge of the flux rope where the axial magnetic field is zero, e.g. Akhavan-Tafti et al., 2018; Burlaga et al., 1988; Lepping et al., 1990; Slavin et al., 2003). B_0 and the impact factor (IP) are both unknowns. The normalized impact factor is a measure of how close the spacecraft crossed to the FTE core and is in dimensions of flux rope radii (R_{FR}), with 0 signifying that the spacecraft crossed through the center of the flux rope and 1 being the edge of the flux rope. IP was estimated from a χ^2 least-squares minimization, and B_0 was then scaled accordingly from the observations (see Slavin et al., 2003 for more details). The measurements for the axial direction, B_A , are in the intermediate direction, while the tangential direction B_T are from the minimum and maximum MVA vector directions, and where fit geometrically. This method has been used previously by Jasinski, Slavin et al. (2016) as well as at Earth studies such as Akhavan-Tafti et al. (2018). We refer the reader to Akhavan-Tafti et al. (2018) for an in-depth description of the method.

An example of the model that was fit to an FTE observation is shown in Figures 3c–3e. The model is in blue compared to the data in black. It can be seen that the structural shape of the force-free flux rope model is well represented in the data. This provides evidence that this particular FTE flux rope (04-Feb-2007), is close to being in the force-free state.

2.5. Magnetic Flux Content Estimation

The magnetic flux content (Φ) of each FTE is calculated using:

$$\Phi = \frac{2\pi}{\alpha} B_0 R_{FR}^2 J_1(\alpha) \quad (4)$$

To estimate the magnetic flux content of each FTE, the velocity of the flux rope passing over the spacecraft requires estimation, and then, using the transit time, we calculate the size of the FTE (i.e. R_{FR}). To do this we use the estimated velocity of the plasma from CAPS-IMS observations. We use the calculated moments that are presented in the PDS (link in acknowledgments), using the velocities estimated for protons. The PDS data presents a quality flag for the plasma measurements with three levels of quality—(1) “Not-Bad”: corotation direction is in the FOV; (2) “Not-Bad”: corotation direction is not in the FOV; and (3) “Bad”: spacecraft is rolling or CAPS is not actuating. We take extra precaution when the quality is listed as “Bad”—and therefore for August 30, 2008 we give a range for the possible velocity centered on the estimate available from PDS. The range is based on a liberal error of 50% and is therefore 200 ± 100 km/s. The estimated flux content for each FTE is listed in Table 2.

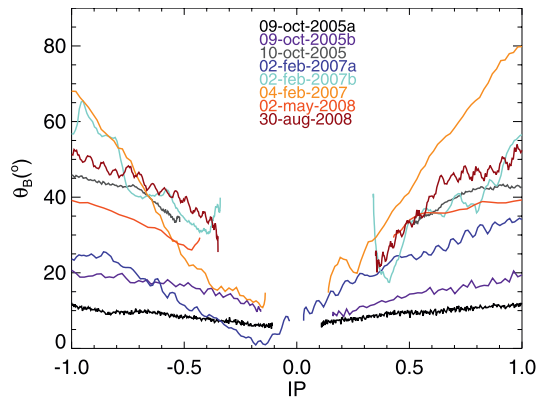


Figure 4. Twisting of the FTE. We estimate the level of twisting of the magnetic field as a ratio of the tangential and axial components of the magnetic field inside the FTE (θ_B). This is shown as a function of impact factor (IP). See text in Section 2.5 for more details.

The errors associated with the estimation of the size, and flux content of these FTEs are considerably large. The size is dependent on velocity moment calculations which due to the lack of full 4π measurements results in the ion moments that are very dependent on look direction. We therefore advise caution in interpreting these values and indicate that these are order of magnitude estimates.

2.6. Analyzing the Level of Twisting of the Magnetic Field inside the FTEs

We estimate the twisting of the magnetic field θ_B , inside the FTE as a ratio of the tangential and axial components of the magnetic field inside the FTE, i.e. $\theta_B = \tan^{-1}(B_T / B_A)$. This is estimated as a function of the impact parameter (IP). In Figure 4, we differentiate the leading and trailing sides (i.e. the entry and exit points of the FTE by the spacecraft, respectively) of the FTE by negative and positive IP values, respectively. Each FTE is shown individually by a separate color. θ_B shows how the core (i.e. axial) component of the FTE magnetic field becomes more

dominant at the center of the FTE, and the tangential component is larger to toward the edges. There isn't a significant difference in θ_B between the leading and trailing sections of the FTE, except for possibly the 04-Feb-2007 FTE (orange line), where θ_B is greater on the trailing side. This analysis is very dependent on the exact trajectory of the spacecraft through the FTE, the FTE shape (which will not be perfectly cylindrical), as well as the velocity. However, generally this shows that the FTE magnetic structures at Saturn are mostly symmetric.

2.7. Electron Measurements inside the FTEs

Using ELS data, we compared the electron energy distributions inside the FTEs and for the accumulation times outside the FTE, directly adjacent to the FTE. Due to the IMS accumulation time being 32 s (longer than FTE durations), we did not do this analysis for the ion measurements because any evidence for energization may be lost due to the averaging of the data inside and outside the FTE in a single accumulation.

ELS has a shorter averaging time (of 8 s) than IMS, and therefore we were able to analyze data separately inside the FTE. Due to the ELS instrument being mounted on a moving actuator, the FOV and therefore the pitch angle (PA) coverage of each of the instrument's eight anodes varies from accumulation to accumulation. Therefore, in the analysis we compare data from individual anodes that shared similar PA coverage. An example of this can be seen in Figure 5, which shows the perpendicular (PERP) and quasi-anti-parallel (APAR) pitch angle measurements for the 10-Oct-2005 FTE. We show the electron phase space density (PSD) measurements immediately before the FTE crossing, during the FTE and immediately after. "Before" the FTE corresponds to a measurement adjacent to the "leading" edge of the FTE, while "after" corresponds to the measurements adjacent to the "trailing" edge of the FTE. Different anodes are used to compare to each other so that measurements for a similar pitch angle can be compared. Unfortunately, an electron comparison for all three pitch angle directions (i.e. 0° , 90° , and 180°) is not available for any of the FTEs. For 02-Feb-2007b and 30-Aug-2008, two directions are available but not for all three bins (i.e. inside FTE and two adjacent bins).

The results can be seen in Figures 5a and 5b which shows two electron measurements inside the FTE (red and green). For perpendicular pitch angles, there is no difference in the electron energy PSD distribution inside and outside the FTE. However, it can be seen that the trailing half of the FTE observation has an enhancement (labeled by green arrow) at higher energies in the quasi-anti-parallel direction during the FTE (at ~ 1 keV; green line). This energization is not observed upon leaving ("after") the FTE which shows that this energization is taking place inside the FTE, and that the energized electrons are streaming along the magnetic field. Although it should be noted that, the measurement for the enhanced electrons (green line) has a larger spread in pitch angle, and therefore there will be a small contribution from electrons with

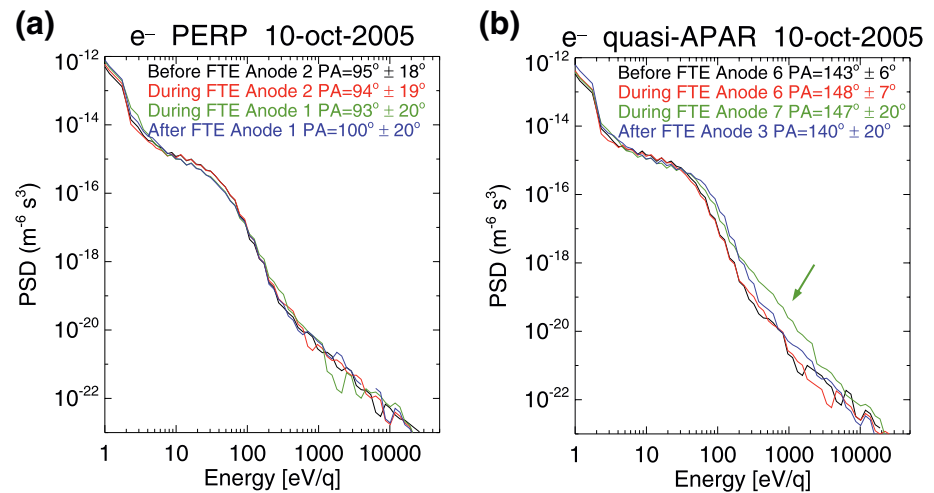


Figure 5. Phase space density (PSD) distributions for electron measurements for the 10-Oct-2005 FTE. The distributions are shown for before (black), during (red and green) and after (blue) the FTE, for two pitch angle directions, perpendicular ('PERP'-left) and quasi-anti-parallel ('quasiAPAR'-right).

slightly higher pitch angles. The CAPS-ELS pitch angle coverage to investigate this at the other FTEs is only suitable at the 09-Oct-2005a and 02-Feb-2007b and 30-Aug-2008 FTEs, where the instrument could sample both 90° as well as one of either 0° or 180° pitch angles. For 09-Oct-2005a and 02-Feb-2007b there is evidence for energization of electrons flowing in the quasi- 0° and quasi- 180° respectively, while no evidence is seen for 30-Aug-2008. This analysis therefore shows there is energization of electrons inside the FTEs (except for 30-Aug-2008).

2.8. Magnetopause Plasma Observations and Analysis of Streaming Electrons

Similar to Fuselier et al. (2014, 2020), we analyzed the magnetopause crossings for streaming electrons in the magnetosheath which provide evidence that reconnection is taking place at the magnetopause locally to the spacecraft. Figure 6 shows plasma observations for a magnetopause crossing (02-May-2008) where an FTE was observed. Figure 6a shows energetic electrons observed by LEMMS. Figures 6b–6e show energy-time spectrograms from ELS measurements for different pitch angles. For this particular time period we do not have full pitch angle coverage, with a lack of coverage at a pitch angle of 0° . We therefore present quasi-parallel measurements for a pitch angle bin of 26° – 51° (Figure 6b). Figure 6c shows electrons at perpendicular pitch angles (77° – 103°). Figures 6d and 6e shows quasi-anti-parallel (129° – 154°) and antiparallel (154° – 180°) electron measurements, respectively. In the magnetosphere, before entering the magnetopause current layer at $\sim 15:37$ UT, the electrons are higher in energy ($\sim 1,000$ eV in ELS) and have higher fluxes at the observed quasiparallel and antiparallel pitch angles, when compared to the perpendicular direction.

Once Cassini is in the magnetosheath, ELS continues to observe the magnetospheric electron population as evidenced by the higher fluxes at higher energies ($\sim 1,000$ eV), at the quasi-anti-parallel and the antiparallel pitch angles. This is in comparison to the perpendicular direction, which largely measures high fluxes only at magnetosheath energies of ~ 100 eV. The observation of heated streaming electrons in the magnetosheath suggests evidence of reconnection and an open magnetopause, where magnetosheath electrons have been heated due to reconnection at the magnetopause (e.g. Fuselier et al., 2014; McAndrews et al., 2007). Streaming electrons have been used in various studies to understand the open magnetopause at Saturn (e.g. Badman et al., 2013; Fuselier et al., 2014, 2020; McAndrews et al., 2008; Sawyer et al., 2019), as well as at Earth (e.g. Fuselier et al., 1997, 2012; Gosling et al., 1990). A summary of this analysis for the magnetopause observations at the FTEs is listed in Table 3. The pitch angle (PA) coverage of ELS is shown as well as the direction where streaming electrons were observed. We find that for all the FTEs except for 30-Aug-2008, there are plasma signatures showing evidence for an open magnetopause during the time of our FTEs.

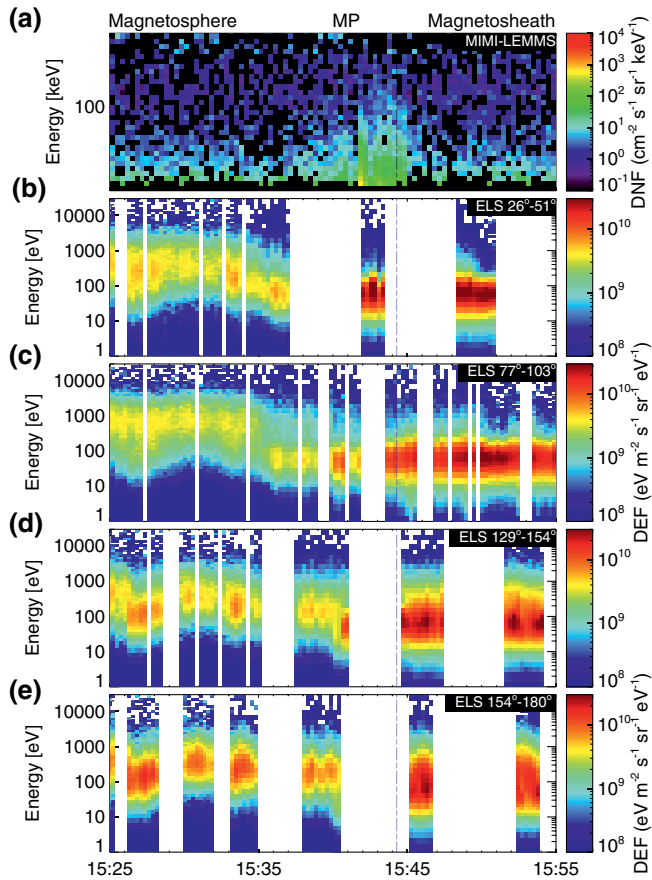


Figure 6. Plasma observations for the magnetopause (MP) crossing on 02-May-2008. Panel (a) shows higher-energy electron measurements from the LEMMS instrument (fluxes shown in differential number flux—DNF). Panels (b)–(e) are directional measurements of lower-energy electrons by CAPS-ELS (in differential energy flux—DEF); (b) shows quasi parallel electron fluxes, (c) shows perpendicular electron fluxes; (d) shows quasi antiparallel electron fluxes and (e) antiparallel electron fluxes. The corresponding pitch angle bin is shown in the top right corner of each individual panel for ELS. The dashed line shows the location of the FTE observation.

2.9. Assessment of Magnetopause Conditions with Respect to Reconnection

We analyzed the magnetopause conditions with respect to reconnection suppression (described in the introduction). A large difference in plasma- β acts to suppress the magnetopause from reconnection if the magnetic shear across the magnetopause is not antiparallel (i.e. $<180^\circ$). Figures 7a–7c shows this analysis for a magnetopause crossing on 10-Oct-2005. Cassini crossed from the magnetosheath into the magnetosphere. Figure 7a shows the magnetic field measurements from MAG and Figure 7b shows data from ELS. The magnetopause current layer (MPCL) was selected where there is a clear rotation from a magnetospheric orientation (i.e. in the θ direction), as well as a change in the plasma properties (lower-energy and higher fluxes in the magnetosheath in comparison to higher-energy and lower fluxes in the magnetosphere). Figure 7c shows the magnetic pressure (gray) from MAG and plasma pressure moment estimations from CAPS as well as MIMI. ELS pressures are shown in black, while IMS pressures are shown for protons (blue) and ions with a mass-per-charge ratio of 2 (i.e. H_2^+ and He^{++} ; red). Also shown is the high-energy (“High-E”) plasma pressure component measured by MIMI (green). Using the magnetic and plasma pressures we can then estimate the plasma- β (i.e. the plasma to magnetic pressure ratio) by taking averages of 1, 5, 10, and 15 min for MAG, ELS, MIMI, and IMS data, respectively (method previously used by Masters et al., 2012 and Jasinski, 2015). The plasma- β for this magnetopause crossing is shown to be ~ 4 in the magnetosheath and ~ 1 in the magnetosphere. We do not use pressure estimates for thermal water-group ion (W+) measured by IMS, because there were not enough data available to make reliable moment estimations for these heavy species. However, in a survey of plasma- β at Saturn’s magnetopause (using this method) Masters et al. (2012) found that the estimation of plasma- β is not sensitive to W+ moments, and accounts for less than 10% of the magnetospheric plasma pressure. We also do not use data from 30-Aug-2008 since the moments are flagged as “Bad” (as described above). A summary of the results for the other magnetopause crossings are shown in Table 3.

The theory of diamagnetic suppression suggests that reconnection is suppressed when the following condition is satisfied:

$$|\Delta\beta| > \frac{2L}{d_i} \tan\left(\frac{\Theta}{2}\right) \quad (5)$$

Table 3
Analysis of Magnetopause Conditions Including Evidence of Streaming Electrons and Plasma- β Estimations

FTE date	Msh d_i (km)	PA coverage ($^\circ$)	Heated e^- ?	MPCL (time)	MSh- β	MSp- β	$ \Delta\beta $	Shear ($^\circ$)
09-Oct-2005 (a,b)	644	0, 90	Yes 0°	17:23:00–17:33:30	24.5	1.0	23.5	124
10-Oct-2005	498	90, 180	Yes 180°	06:06:45–06:10:00	3.8	1.1	2.7	111
02-Feb-2007 (a)	441	0,90,180	Yes 180°	11:26:16–11:26:29	47.0	1.2	45.8	153
02-Feb-2007 (b) *	516 ^a	0,90,180	Yes 180°	23:29:00–23:44:18	16	0.3	15.7	155
04-Feb-2007	639	0,90	Yes 0°	11:07:00–11:13:00	1.8	0.3	1.5	141
02-May-2008	671	90,180	Yes 180°	15:35:30–15:45:30	1.8	0.8	1.0	99
30-Aug-2008	361	0,90,180	No	10:10:00–10:11:10	–	–	–	52

^aThis length is estimated from density measurements at the FTE, since the magnetosheath (“Msh”) is crossed later.

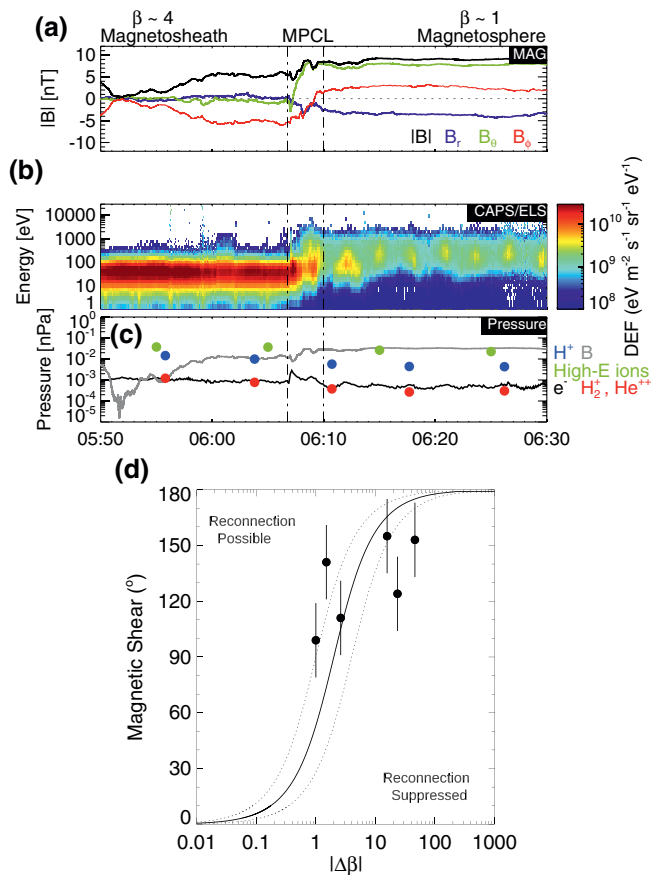


Figure 7. Assessment of the magnetopause conditions at observed FTEs in regards to diamagnetic suppression of magnetic reconnection. Top: example of the magnetic shear and plasma- β estimation on 10-Oct-2005; data shown as a timeseries. The dashed vertical line shows the location of the magnetopause current layer (MPCL) including the magnetic field rotation and change in plasma conditions. Panel (a) shows the magnitude (black) and the three components (colored) of the magnetic field measurements by MAG. Panel (b) shows the electron flux measured by CAPS-ELS (background removed). Panel (c) shows the magnetic (gray) and plasma (colored dots) pressure estimation, with the resulting plasma- β calculation labeled for the magnetosphere and magnetosheath. Bottom: panel (d) shows the summary of the results for all the FTEs. The black line shows the theoretical boundary (Equation 5) between where reconnection is possible and is suppressed, for a current sheet thickness of $L = 1 d_i$, while the dotted lines are for L equal to $0.5 d_i$ and $2 d_i$ (where d_i is the ion inertial length).

where $\Delta\beta$ is the difference in plasma- β across the magnetopause, L is the width or thickness of the magnetopause current layer (i.e. the density gradient layer) and d_i is the ion inertial length, and Θ is the magnetic shear across the MPCL. To estimate d_i in the magnetosheath, we use Thomsen et al. (2018)—who completed a survey of magnetosheath plasma properties using CAPS data—and use an average of the electron density measured by ELS and the proton density measured by IMS.

Figure 7d shows the plasma- β and magnetic shear conditions at the magnetopause for the magnetopause crossings during which an FTE was observed. Equation 5 shows the expression for the theoretical boundary between “reconnection suppressed” and “reconnection possible” conditions and is shown as the black line for a current sheet thickness of $L = 1 d_i$, and as dotted lines for $L = 0.5$ and $2 d_i$ (Figure 7d). Half the observations occur in the theoretically “reconnection possible” regime. Given the uncertainties associated with estimating $\Delta\beta$, as discussed by Masters et al. (2012), this may not be the most accurate test of diamagnetic suppression of reconnection proposed by Swisdak et al. (2003). Furthermore, the magnetic shear is given as a 20° uncertainty as described by Fuselier et al. (2014). When using the pressure moments which are considered “Not-bad,” we can see that FTEs all lie on magnetopause (MP) boundaries where the conditions are close to the theoretical boundary of being possible (and not suppressed). However, considering the low estimated magnetic shear angle for 30-Aug-2008, it is very likely that this event would lie in the suppressed regime, considering how the typical magnetosheath plasma- β value is ~ 10 (Masters et al., 2012).

3. Discussion

In this paper we have presented the discovery of seven new FTE flux ropes at Saturn’s dayside magnetopause. Including the FTE flux rope reported by Jasinski, Slavin et al. (2016), we have analyzed together all eight known FTEs at Saturn’s dayside magnetopause. The process of multiple x-line reconnection is considered the generation mechanism for FTEs (e.g. Lee & Fu, 1985; Raeder, 2006), and FTEs have been widely studied at Earth and Mercury (e.g. Akhavan-Tafti et al., 2019; Slavin et al., 2012). However, the magnetopause conditions at the outer planets differ vastly from the inner planets as the solar wind expands radially outwards throughout the heliosphere. Therefore, it is important to understand—through observations—how this process differs at an outer planet magnetosphere such as at Saturn’s, using plasma instrumentation onboard the Cassini spacecraft.

Using MVA and force-free flux rope modeling, we analyzed the structure of each of the FTEs. All the FTEs featured bipolar signatures in the B_{MAX} component of the magnetic field, as well as peaks at closest approach to the FTE core in the B_{INT} direction. These are typical FTE signatures seen at Earth and Mercury. The vector direction of INT shows the direction of the axial field and consequently the orientation of the expected reconnection x-line at the magnetopause (shown in Table 2). As is mostly expected, the core direction (shown in Table 2) for most of the FTEs is in the azimuthal (ϕ_{KRTP}) direction as would be expected from quasi-antiparallel reconnection (i.e. a magnetic shear close to 180°). However, not all of the FTEs are orientated in this expected direction, most notably (and most interestingly) the FTEs observed on 02-Feb-2007a and 20-Aug-2008, which have their core axis aligned in the R_{KRTP} and θ_{KRTP} directions, respectively. For 02-Feb-2007a, this may be somewhat explained by the fact that this FTE was observed at the high southern latitude of -38° , and therefore the axis of this FTE had rotated from its original orientation while convecting away from the subsolar magnetopause where it

was likely generated. This occurred due to magnetic tension which caused the FTE to “straighten” toward higher latitudes. For 30-Aug-2008, the orientation of the x-line and therefore FTE in the θ_{KRTP} direction is not unexpected considering the magnetic shear at the magnetopause at this time was estimated to be $\sim 52^\circ$. With such a low shear angle, if reconnection were to take place, the x-line would most likely be rotated away from the azimuthal direction toward the observed direction, similar to low-shear reconnection that has been observed at Mercury (e.g. Slavin et al., 2012, 2014). Whether or not this is the case for this particular event is not certain, considering that the FTE could have been generated elsewhere along the magnetopause under different conditions, as well as the fact that the general conditions at Saturn’s magnetopause are not favorable for low-shear reconnection (Masters et al., 2012). However, both pieces of evidence (core direction and magnetopause shear) agree and indicate that this may have occurred.

The 09-Oct-2005b FTE also presented an unusual core direction. This particular FTE is the smallest of the group reported here and is subion in scale. For such small FTEs, turbulence will become important and plays a significant role in reconnection and will affect and vary the 2D description of this process. Daughton et al. (2011) report the simulation of small-scale FTEs which have axes that are clearly deviated from what we would expect in our 2D approximation for larger FTEs.

3.1. FTE Size and Growth Mechanism

There is a variation in the estimated size of the various FTEs. The size ranges from 534 km to 14,040 km. This is similar to Earth observations; a survey of 1,034 FTEs (Fermo et al., 2011; Wang et al., 2005) observed by the Cluster mission between 2001 and 2003 found FTE sizes at Earth of 1,000–25,000 km, with an exponential fit of 5,300 km (Akhavan-Tafti et al., 2018). Analysis of 55 FTEs by the MMS mission at Earth found FTE sizes of 500–8,000 km, with a nominal size of 1700 km (Akhavan-Tafti et al., 2018), similar to the sizes found at Saturn’s magnetopause of 534–14,040 km. The size with respect to the ion inertial length (d_i) differs between the magnetosheaths of Earth and Saturn. At Earth, d_i is lower than at Saturn at the magnetopause, and approximately found to be ~ 50 km for the observations of the MMS FTEs, which results in terrestrial FTE sizes reported by Akhavan-Tafti et al. (2018) of $30 d_i$ or greater. Due to the lower densities at Saturn’s dayside magnetosheath, d_i is greater and is on average 501 km (estimated by taking the average proton and electron densities obtained from the magnetosheath survey at Saturn by Thomsen et al. 2018). The FTEs reported in this paper range in size from a d_i in diameter to several d_i (largest two FTEs being 10 and 27 d_i in diameter). Therefore, the FTEs observed at Saturn are ion-scale flux ropes, and are similar to the small ion-scale FTEs that have been observed at Earth and reported by Eastwood et al. (2016).

From the present study we cannot determine the exact process that causes FTE growth in the larger FTEs that were detected at Saturn. Observations as well as kinetic and magnetohydrodynamic simulations have shown that FTEs at Earth usually grow at the subsolar point as they convect down the magnetopause away from the initial reconnection site (e.g. Dorelli & Bhattacharjee, 2009; Eastwood et al., 2012; Hoilijoki et al., 2017). This can be caused by three different mechanisms. Adiabatic expansion causes the FTE to grow due to a pressure imbalance between FTE and the surrounding magnetosheath. As the FTE moves away from the subsolar point, the pressure in the magnetosheath reduces causing the FTE to grow (e.g. Akhavan-Tafti et al., 2019). Continuous x-line reconnection will grow the FTE by continuously adding magnetic flux to the initially formed magnetic island (e.g. Raeder, 2006). Finally, coalescence, is the growth of FTEs by merging and subsequent reconnection of a chain of smaller ion-scale flux ropes (e.g. Akhavan-Tafti et al., 2020; Biskamp, 1982; Hwang et al., 2018; Zhou et al., 2017). The symmetric structure of the FTE twisting (shown in Figure 4) may indicate that from these three mechanisms, coalescence is less likely, as it would grow an FTE that is asymmetric (as a larger FTE would have merged with a smaller FTE). From the remaining two mechanisms it is highly probable that adiabatic expansion may be the only viable candidate for FTE growth at Saturn (if the FTEs grow at all at Saturn’s magnetopause).

Due to the diamagnetic suppression of reconnection at Saturn, both reconnection mechanisms (continuous reconnection and coalescence) are unlikely to be dominant. This may mean that with limited FTE generation and growth mechanisms, FTEs are more likely to be very small in d_i in comparison to those observed at Mercury and Earth. We therefore suggest that although there are now eight reported FTE crossings at Saturn, there may well be many more FTEs that have simply been overlooked due to their small size and therefore brief and unremarkable magnetic signatures. FTEs forming at the ion-scale may not grow, due to a

lack of the main growth mechanisms. Instead at Saturn there may be a “drizzle” of very small FTEs of $\sim 1 d_i$ in diameter that remain undetected. A serious automated effort is therefore required to investigate whether this is the case at Saturn’s magnetopause.

3.2. FTE Magnetic Flux Content and Contribution to Flux Transfer at Saturn’s Magnetosphere

The 02-Feb-2007b FTE reported by Jasinski, Slavin et al. (2016) is the largest FTE observed at Saturn and possesses the highest magnetic flux content of all the FTEs reported here. With a magnetic flux content of ~ 460 kWb, it is similar to terrestrial FTEs with previously reported flux contents $\sim 10^2$ kWb (e.g. Lui et al., 2008; Zhang et al., 2008). However, from this investigation, most of the measured FTEs at Saturn are much smaller in magnetic flux content ranging $1\text{--}10^2$ kWb. Taking the largest magnetic flux content estimated for the 02-Feb-2007b FTE of 0.46 MWb (also assuming the five traveling compression regions reported by Jasinski, Arridge et al., 2016 were also FTEs) and comparing it to the average change in open flux calculation of ~ 7 GWb during a Dungey cycle from Badman et al. (2014), this would mean that FTEs account for less than 0.1% of the opening of flux. This is the largest FTE, and therefore it is most likely an uncommon occurrence. Even if there are many small FTEs present in the Cassini data that have not been accounted for, it would require an unrealistic number of small FTEs to contribute even 1% of the 7 GWb of opened flux mentioned above and therefore small FTEs would most likely result in negligible flux transfer at Saturn’s magnetosphere. This is in contrast to Earth, where FTEs may be a considerable means of driving the Dungey cycle (e.g. Fear et al., 2017; Lockwood et al., 1995; Milan et al., 2000). At Mercury, it is expected that FTEs transport enough flux to drive Mercury’s Dungey cycle (Fear et al., 2019). Therefore, FTEs at Saturn do not account for any significant amount of open flux transferred at Saturn’s magnetosphere, and that this process is largely negligible at this Giant Magnetosphere.

3.3. Plasma Acceleration inside FTEs

The ion measurements from IMS do not have a sufficiently high enough time resolution to explore ion acceleration inside the FTEs. There are however, measurements of the acceleration of electrons inside of the FTEs along the magnetic field. Acceleration of plasmas can occur along reconnecting magnetic field lines due to different mechanisms. This can be described as an equation for the rate of kinetic energy (W) gain of particles in the guiding center limit where the first adiabatic invariant is conserved (Drake et al., 2019):

$$\frac{dW}{dt} = E_{\parallel} J_{\parallel} + \frac{P_{\perp}}{B} \left(\frac{\partial B}{\partial t} + \mathbf{v}_E \cdot \nabla \mathbf{B} \right) + \left(P_{\parallel} + \rho v_{\parallel}^2 \right) \mathbf{v}_E \cdot \boldsymbol{\kappa} \quad (6)$$

The first term on the right side is the acceleration of particles due to parallel electric fields ($E_{\parallel} J_{\parallel}$). The second term shows Betatron acceleration which is the perpendicular change in energy due to the first magnetic moment, where P_{\parallel} and P_{\perp} are the parallel and perpendicular pressures, and \mathbf{v}_E is the $\mathbf{E} \times \mathbf{B}$ drift velocity. Betatron acceleration could be important in the reconnection outflow region due to magnetic flux pile up as suggested by simulations (Ashour-Abdalla et al., 2011; Dahlin et al., 2014) and observations (Akhavan-Tafti, Slavin, Sun et al., 2019). Betatron acceleration would normally cause the enhancements of perpendicular pitch angles (i.e. 90°) in particle distributions. However, this was not the case for the present study, which might indicate that the Betatron acceleration is less important. The third term is the Fermi acceleration process, where ρ and v_{\parallel} are the mass density and parallel bulk velocity, respectively, and the curvature is $\boldsymbol{\kappa} = (\mathbf{B} \cdot \nabla) \mathbf{B} / B^2$; this process occurs due to the straightening of magnetic field lines due to the magnetic tension force, and acts to accelerate particles parallel to the magnetic field. The enhancements of electron flux in the quasi-anti-parallel direction ($\sim 150^\circ$, for example, the case in Figure 5) could be evidence of Fermi acceleration. However, since there is a lack of measurements along the quasiparallel direction, and the Fermi acceleration normally would result in acceleration both in parallel and antiparallel directions, more comprehensive electron and ion measurements would be needed to understand the importance of this acceleration mechanism.

It is the first term (parallel electric fields), which has been found to be the most dominant acceleration process, and is largely responsible for energizing particles at Earth during reconnection (Egedal et al., 2012) and has been found to account for most of the energization of electrons inside FTEs in a survey of MMS

spacecraft FTE observations (Akhavan-Tafti, Slavin, Sun et al., 2019). Cassini plasma-measurement data are not as detailed as those made by the MMS mission at Earth, and therefore we cannot conclude what the exact process is for the cause of plasma energization at FTEs at Saturn's magnetopause. Neither can we understand detailed plasma structure within the FTEs. Due to the measurement of energized electrons at quasi-field-aligned pitch angles, we can only conclude that the processes responsible for this could be Fermi acceleration or parallel electric fields, or a combination of the two.

3.4. Diamagnetic Suppression of Reconnection at Saturn's Magnetopause

We explored the conditions of Saturn's magnetopause during our FTE crossings to understand flux rope generation in the context of diamagnetic suppression of reconnection. The solar wind at the outer planets has a higher magnetosonic Mach number in comparison to the inner solar system, therefore, magnetosheaths at the outer planets will have a higher plasma- β . The higher plasma- β in the magnetosheath means that the change in plasma- β across the magnetopause will be much larger resulting in a drift of charged particles within the magnetopause current layer, which disrupt reconnection jets. The larger variation of plasma- β subsequently acts to suppress reconnection from occurring unless the magnetic shear between the two fields is antiparallel, that is 180° (e.g. Masters, 2015, 2018; Masters et al., 2012; Paschmann et al., 1986; Phan et al., 2010; Quest & Coroniti, 1981; Scurry et al., 1994; Swisdak et al., 2003, 2010).

The observed FTEs occurred at magnetopause boundary conditions which were either conducive to reconnection or close to the theoretical boundary between where reconnection is possible/suppressed (Figure 7d). Of course, the FTE may have been generated under different magnetopause conditions and may have convected along the magnetopause to a new location to be observed by Cassini. We also investigated the electron data for evidence of reconnection signatures in the magnetosheath, similar to the investigation of Fuselier et al. (2014, 2020). We found field-aligned magnetospheric electrons in the magnetosheath which shows evidence of reconnection locally at the magnetopause crossing (at all our FTEs except for the 08-Aug-2008).

There is evidence from simulations (i.e. Raeder, 2006) and observations (i.e. Hasegawa et al., 2008) that the conditions for FTE generation require component reconnection (i.e. reconnection which is not antiparallel and therefore magnetic shears of $<180^\circ$), and occurs during "sequential x-line reconnection." This would explain the significant amounts of FTEs generated and observed at Earth and Mercury where evidence of low-latitude reconnection has been found for shear angles as low as 50° (Trattner et al., 2017) and 27° (Slavin et al., 2014), respectively. Since component reconnection is more likely to be suppressed at Saturn, this would reconcile the small number of FTEs at Saturn's magnetopause in comparison to the larger amount of other reconnection signature observations reported and described in the introduction (i.e. Badman et al., 2013; Fuselier et al., 2020; Jasinski et al., 2014, etc.). This does not however dismiss the previously mentioned hypothesis that there may more FTEs with much smaller sizes left to be discovered in the Cassini data set – if the generation and growth mechanisms are suppressed, this may result in fewer and smaller FTEs in comparison to Earth, but more than the current 8 FTEs discovered in the 13-year Cassini data set. This is also supported by recent modeling efforts that generally found lower FTE generation rates for higher solar wind Mach numbers as well as a higher proportion of FTEs with lower field magnitudes (Chen et al., 2019); meaning that smaller FTEs may be more common at a magnetopause such as Saturn's.

4. Conclusions

We have reported the discovery of seven new FTE-type flux ropes at Saturn's magnetopause. Including the FTE reported by Jasinski, Slavin et al. (2016) we have analyzed all 8 FTEs to have been detected at Saturn. From this analysis we present the following conclusions:

1. The FTEs generated at Saturn's dayside magnetopause are on the order of a few ion inertial lengths in diameter and are therefore ion-scale in size
2. We suggest that since the main growth mechanisms for FTEs are most likely suppressed at Saturn (continuous reconnection and coalescence), FTEs at Saturn will remain at the $\sim 1 d_i$ scale, and that there may be a "drizzle" of FTEs occurring that are not obviously detected due to their brief and unobvious magnetic signature

3. Electrons are observed to be energized inside the FTE at quasi-field-aligned pitch angles. The exact process (Fermi acceleration or parallel electric fields) responsible for this could not be determined due to a lack of full pitch angle coverage and high-time-resolution measurements
4. The magnetic flux content of the FTEs is estimated to be $1\text{--}10^2$ kWb. This is very small in comparison to the amount of magnetic flux expected to be opened by dayside reconnection at Saturn. Therefore, flux transfer events at Saturn aren't expected to transfer significant amount of flux at Saturn in comparison to the magnetospheres of Mercury and Earth

Single spacecraft measurements, with low time-resolution plasma instrumentation are not sufficient enough to completely understand how flux ropes are generated at a high plasma- β magnetosheath where reconnection is most likely to be suppressed. Future work will involve running particle-in-cell simulations under various plasma- β conditions to be able to compare flux ropes and their generation at Saturn in comparison to Earth and Mercury.

Data Availability Statement

All the data used in this study can be found at NASA's Planetary Data System (<https://pds.jpl.nasa.gov>).

Acknowledgments

J. M. Jasinski was supported by an appointment to the NASA Postdoctoral Program at the Jet Propulsion Laboratory administered by Universities Space Research Association (USRA) through a contract with the National Aeronautics and Space Administration (NASA). J. M. Jasinski and N. Murphy acknowledge support from the Jet Propulsion Laboratory, California Institute of Technology, under a contract with NASA, and also acknowledge support of the NASA-ROSES Cassini Data Analysis Program (grant number 80NM0018F0612). A. J. Coates acknowledges STFC support via the solar system consolidated grant to UCL-MSSL.

References

- Akhavan-Tafti, M., Palmroth, M., Slavin, J. A., Battarbee, M., Ganse, U., Grandin, M., et al. (2020). Comparative analysis of the Vlasiator simulations and MMS observations of multiple X-line reconnection and flux transfer events. *Journal of Geophysical Research: Space Physics*, *125*, e2019JA027410. <https://doi.org/10.1029/2019JA027410>
- Akhavan-Tafti, M., Slavin, J. A., Eastwood, J. P., Cassak, P. A., & Gershman, D. J. (2019). MMS multi-point analysis of FTE evolution: Physical characteristics and dynamics. *Journal of Geophysical Research: Space Physics*, *124*, 5376–5395. <https://doi.org/10.1029/2018JA026311>
- Akhavan-Tafti, M., Slavin, J. A., Le, G., Eastwood, J. P., Strangeway, R. J., Russell, C. T., et al. (2018). MMS examination of FTEs at the Earth's subsolar magnetopause. *Journal of Geophysical Research: Space Physics*, *123*, 1224–1241. <https://doi.org/10.1002/2017JA024681>
- Akhavan-Tafti, M., Slavin, J. A., Sun, W. J., Le, G., & Gershman, D. J. (2019b). MMS observations of plasma heating associated with FTE growth. *Geophysical Research Letters*, *46*, 12654–12664. <https://doi.org/10.1029/2019GL084843>
- Arridge, C. S., Jasinski, J. M., Achilleos, N., Bogdanova, Y. V., Bunce, E. J., Cowley, S. W. H., et al. (2016). Cassini observations of Saturn's southern polar cusp. *Journal of Geophysical Research: Space Physics*, *121*, 3006–3030. <https://doi.org/10.1002/2015JA021957>
- Arridge, C. S., McAndrews, H. J., Jackman, C. M., Forsyth, C., Walsh, A. P., Sittler, E. C., et al. (2009). Plasma electrons in Saturn's magnetotail: Structure, distribution and energisation. *Planetary and Space Science*, *57*(14–15), 2032–2047. <https://doi.org/10.1016/j.pss.2009.09.007>
- Ashour-Abdalla, M., El-Alaoui, M., Goldstein, M., Zhou, M., Schriver, D., Richard, R., et al. (2011). Observations and simulations of non-local acceleration of electrons in magnetotail magnetic reconnection events. *Nature Physics*, *7*, 360–365. <https://doi.org/10.1038/nphys1903>
- Badman, S. V., Jackman, C. M., Nichols, J. D., Clarke, J. T., & Gérard, J.-C. (2014). Open flux in Saturn's magnetosphere. *Icarus*, *231*, 137–145. <https://doi.org/10.1016/j.icarus.2013.12.004>
- Badman, S. V., Masters, A., Hasegawa, H., Fujimoto, M., Radioti, A., Grodent, D., et al. (2013). Bursty magnetic reconnection at Saturn's magnetopause. *Geophysical Research Letters*, *40*, 1027–1031. <https://doi.org/10.1002/grl.50199>
- Biskamp, D. (1982). Effect of secondary tearing instability on the coalescence of magnetic islands. *Physics Letters A*, *87*(7), 357–360. [https://doi.org/10.1016/0375-9601\(82\)90844-1](https://doi.org/10.1016/0375-9601(82)90844-1)
- Burlaga, L. F. (1988). Magnetic clouds and force-free fields with constant alpha. *Journal of Geophysical Research*, *93*(A7), 7217–7224. <https://doi.org/10.1029/JA093iA07p07217>
- Chen, C., Sun, T. R., Wang, C., Huang, Z. H., Tang, B. B., & Guo, X. C. (2019). The effect of solar wind Mach numbers on the occurrence rate of flux transfer events at the dayside magnetopause. *Geophysical Research Letters*, *46*, 4106–4113. <https://doi.org/10.1029/2018GL081676>
- Dahlin, J. T., Drake, J. F., & Swisdak, M. (2014). The mechanisms of electron heating and acceleration during magnetic reconnection. *Physics of Plasmas*, *21*(9), 92304. <https://doi.org/10.1063/1.4894484>
- Daughton, W., Roytershteyn, V., Karimabadi, H., Yin, L., Albright, B. J., Bergen, B., & Bowers, K. J. (2011). Role of electron physics in the development of turbulent magnetic reconnection in collisionless plasmas. *Nature Physics*, *7*(7), 539–542. <https://doi.org/10.1038/nphys1965>
- Dorelli, J. C., & Bhattacharjee, A. (2009). On the generation and topology of flux transfer events. *Journal of Geophysical Research*, *114*, A06213. <https://doi.org/10.1029/2008JA013410>
- Dougherty, M. K., Kellock, S., Southwood, D. J., Balogh, A., Smith, E. J., Tsurutani, B. T., et al. (2004). The Cassini magnetic field investigation. *Space Science Reviews*, *114*, 331–383. <https://doi.org/10.1007/s11214-004-1432-2>
- Drake, J. F., Arnold, H., Swisdak, M., & Dahlin, J. T. (2019). A computational model for exploring particle acceleration during reconnection in macroscale systems. *Physics of Plasmas*, *26*(1), 12901. <https://doi.org/10.1063/1.5058140>
- Dungey, J. W. (1961). Interplanetary magnetic field and the auroral zones. *Physical Review Letters*, *6*, 47–48. <https://doi.org/10.1103/PhysRevLett.6.47>
- Eastwood, J. P., Balogh, A., Dunlop, M. W., & Smith, C. W. (2002). Cluster observations of the heliospheric current sheet and an associated magnetic flux rope and comparisons with ace. *Journal of Geophysical Research*, *107*(A11), 1365. <https://doi.org/10.1029/2001JA009158>
- Eastwood, J. P., Phan, T. D., Cassak, P. A., Gershman, D. J., Haggerty, C., Malakit, K., et al. (2016). Ion-scale secondary flux ropes generated by magnetopause reconnection as resolved by MMS. *Geophysical Research Letters*, *43*, 4716–4724. <https://doi.org/10.1002/2016GL068747>

- Eastwood, J. P., Phan, T. D., Fear, R. C., Sibeck, D. G., Angelopoulos, V., Øieroset, M., & Shay, M. A. (2012). Survival of flux transfer event (FTE) flux ropes far along the tail magnetopause. *Journal of Geophysical Research*, *117*, A08222. <https://doi.org/10.1029/2012JA017722>
- Egedal, J., Daughton, W., & Le, A. (2012). Large-scale electron acceleration by parallel electric fields during magnetic reconnection. *Nature Physics*, *8*, 321–324. <https://doi.org/10.1038/nphys2249>
- Fear, R. C., Coxon, J. C., & Jackman, C. M. (2019). The contribution of flux transfer events to Mercury's Dungey cycle. *Geophysical Research Letters*, *46*, 14239–14246. <https://doi.org/10.1029/2019GL085399>
- Fear, R. C., Milan, S. E., Fazakerley, A. N., Lucek, E. A., Cowley, S. W. H., & Dandouras, I. (2008). The azimuthal extent of three flux transfer events. *Annales Geophysicae*, *26*, 2353–2369. <https://doi.org/10.5194/angeo-26-2353-2008>
- Fear, R. C., Trenchi, L., Coxon, J. C., & Milan, S. E. (2017). How much flux does a flux transfer event transfer?. *Journal of Geophysical Research: Space Physics*, *122*, 12310–12327. <https://doi.org/10.1002/2017JA024730>
- Felici, M., Arridge, C. S., Wilson, R. J., Coates, A. J., Thomsen, M., & Reisenfeld, D. (2018). Survey of thermal plasma composition in Saturn's magnetosphere using time-of-flight data from Cassini/CAPS. *Journal of Geophysical Research: Space Physics*, *123*, 6494–6513. <https://doi.org/10.1029/2017JA025085>
- Fermo, R. L., Drake, J. F., Swisdak, M., & Hwang, K. J. (2011). Comparison of a statistical model for magnetic islands in large current layers with Hall MHD simulations and Cluster FTE observations. *Journal of Geophysical Research*, *116*, A09226. <https://doi.org/10.1029/2010JA016271>
- Fuselier, S. A., Anderson, B. J., & Onsager, T. G. (1997). Electron and ion signatures of field line topology at the low-shear magnetopause. *Journal of Geophysical Research*, *102*(A3), 4847–4863. <https://doi.org/10.1029/96JA03635>
- Fuselier, S. A., Frahm, R., Lewis, W. S., Masters, A., Mukherjee, J., Petrinec, S. M., & Sillanpaa, I. J. (2014). The location of magnetic reconnection at Saturn's magnetopause: A comparison with Earth. *Journal of Geophysical Research: Space Physics*, *119*, 2563–2578. <https://doi.org/10.1002/2013JA019684>
- Fuselier, S. A., Petrinec, S. M., Sawyer, R. P., Mukherjee, J., & Masters, A. (2020). Suppression of magnetic reconnection at Saturn's low-latitude magnetopause. *Journal of Geophysical Research: Space Physics*, *125*(5), e2020JA027895. <https://doi.org/10.1029/2020JA027895>
- Fuselier, S. A., Trattner, K. J., Petrinec, S. M., & Lavraud, B. (2012). Dayside magnetic topology at the Earth's magnetopause for northward IMF. *Journal of Geophysical Research*, *117*, A08235. <https://doi.org/10.1029/2012JA017852>
- Gonzalez, W., & Parker, E. (Eds.). (2016). *Magnetic reconnection: Concepts and applications*. In *Astrophysics and space science library* (Vol. 427, pp. 549). Cham: Springer. Retrieved from <http://cds.cern.ch/record/2136422>
- Gosling, J. T. (2012). Magnetic reconnection in the solar wind. *Space Science Reviews*, *172*, 187–200. <https://doi.org/10.1007/s11214-011-9747-2>
- Gosling, J. T., Thomsen, M. F., Bame, S. J., Onsager, T. G., & Russell, C. T. (1990). The electron edge of the low-latitude boundary layer during accelerated flow events. *Geophysical Research Letters*, *17*, 1833–1836.
- Hasegawa, H., Retinò, A., Vaivads, A., Khotyaintsev, Y., Nakamura, R., Takada, T., et al. (2008). Retreat and reformation of X-line during quasi-continuous tailward-of-the-cusp reconnection under northward IMF. *Geophysical Research Letters*, *35*, L15104. <https://doi.org/10.1029/2008GL034767>
- Hoilijoki, S., Ganse, U., Pfau-Kempf, Y., Cassak, P. A., Walsh, B. M., Hietala, H., et al. (2017). Reconnection rates and X line motion at the magnetopause: Global 2D-3V hybrid-Vlasov simulation results. *Journal of Geophysical Research: Space Physics*, *122*, 2877–2888. <https://doi.org/10.1002/2016JA023709>
- Hwang, K.-J., Sibeck, D. G., Burch, J. L., Choi, E., Fear, R. C., Lavraud, B., et al. (2018). Small-scale flux transfer events formed in the reconnection exhaust region between two X lines. *Journal of Geophysical Research: Space Physics*, *123*, 8473–8488. <https://doi.org/10.1029/2018JA025611>
- Jasinski, J. M. (2015). Cassini observations of Saturn's magnetospheric Cusp (Doctoral thesis). UCL (University College London). Retrieved from <https://discovery.ucl.ac.uk/id/eprint/1470751>
- Jasinski, J. M., Arridge, C. S., Bader, A., Smith, A. W., Felici, M., Kinrade, J., et al. (2019). Saturn's open-closed field line boundary: A Cassini electron survey at Saturn's magnetosphere. *Journal of Geophysical Research: Space Physics*, *124*, 10018–10035. <https://doi.org/10.1029/2019JA027090>
- Jasinski, J. M., Arridge, C. S., Coates, A. J., Jones, G. H., Sergis, N., Thomsen, M. F., & Krupp, N. (2017). Diamagnetic depression observations at Saturn's magnetospheric cusp by the Cassini spacecraft. *Journal of Geophysical Research: Space Physics*, *122*, 6283–6303. <https://doi.org/10.1002/2016JA023738>
- Jasinski, J. M., Arridge, C. S., Coates, A. J., Jones, G. H., Sergis, N., Thomsen, M. F., et al. (2016). Cassini plasma observations of Saturn's magnetospheric cusp. *Journal of Geophysical Research: Space Physics*, *121*, 12047–12067. <https://doi.org/10.1002/2016JA023310>
- Jasinski, J. M., Arridge, C. S., Lamy, L., Leisner, J. S., Thomsen, M. F., Mitchell, D. G., et al. (2014). Cusp observation at Saturn's high-latitude magnetosphere by the Cassini spacecraft. *Geophysical Research Letters*, *41*, 1382–1388. <https://doi.org/10.1002/2014GL059319>
- Jasinski, J. M., Slavin, J. A., Arridge, C. S., Poh, G., Jia, X., Sergis, N., et al. (2016). Flux transfer event observation at Saturn's dayside magnetopause by the Cassini spacecraft. *Geophysical Research Letters*, *43*, 6713–6723. <https://doi.org/10.1002/2016GL069260>
- Kinrade, J., Badman, S. V., Bunce, E. J., Tao, C., Provan, G., Cowley, S. W. H., et al. (2017). An isolated, bright cusp aurora at Saturn. *Journal of Geophysical Research: Space Physics*, *122*(6), 6121–6138. <https://doi.org/10.1002/2016JA023792>
- Knetter, T., Neubauer, F. M., Horbury, T., & Balogh, A. (2004). Four-point discontinuity observations using cluster magnetic field data: A statistical survey. *Journal of Geophysical Research*, *109*(A6), a06102. <https://doi.org/10.1029/2003JA010099>
- Krimigis, S. M., Mitchell, D. G., Hamilton, D. C., Livi, S., Dandouras, J., Jaskulek, S., et al. (2004). Magnetosphere imaging instrument (MIMI) on the Cassini mission to Saturn/Titan. *Space Science Reviews*, *114*, 233–329. <https://doi.org/10.1007/s11214-004-1410-8>
- Lee, L. C., & Fu, Z. F. (1985). A theory of magnetic flux transfer at the earth's magnetopause. *Geophysical Research Letters*, *12*(2), 105–108. <https://doi.org/10.1029/GL012i002p00105>
- Lee, L. C., & Fu, Z. F. (1986). Multiple X line reconnection: 1. A criterion for the transition from a single X line to a multiple X line reconnection. *Journal of Geophysical Research*, *91*(A6), 6807–6815. <https://doi.org/10.1029/JA091iA06p06807>
- Lepping, R. P., Fairfield, D. H., Jones, J., Frank, L. A., Paterson, W. R., Kokubun, S., & Yamamoto, T. (1995). Cross-tail magnetic flux ropes as observed by the GEOTAIL spacecraft. *Geophysical Research Letters*, *22*, 1193–1196. <https://doi.org/10.1029/95GL01114>
- Lepping, R. P., Jones, J. A., & Burlaga, L. F. (1990). Magnetic field structure of interplanetary magnetic clouds at 1 AU. *Journal of Geophysical Research: Space Physics*, *95*(A8), 11,957–11,965. <https://doi.org/10.1029/JA095iA08p11957>
- Liewer, P. C., Panasenco, O., & Hall, J. R. (2013). Stereoscopic analysis of the 31 August 2007 prominence eruption and coronal mass ejection. *Solar Physics*, *282*, 201–220. <https://doi.org/10.1007/s11207-012-0145-z>
- Lockwood, M., Cowley, S. W. H., Smith, M. F., Rijnbeek, R. P., & Elphic, R. C. (1995). The contribution of flux transfer events to convection. *Geophysical Research Letters*, *22*, 1185–1188. <https://doi.org/10.1029/95GL01008>

- Lockwood, M., & Hapgood, M. A. (1998). On the cause of a magnetospheric flux transfer event. *Journal of Geophysical Research*, *103*(A11), 26453–26478. <https://doi.org/10.1029/98JA02244>
- Lui, A. T. Y., Sibeck, D. G., Phan, T., McFadden, J. P., Angelopoulos, V., & Glassmeier, K.-H. (2008). Reconstruction of a flux transfer event based on observations from five THEMIS satellites. *Journal of Geophysical Research*, *113*, A00C01. <https://doi.org/10.1029/2008JA013189>
- Lundquist, S. (1950). Magneto-hydrostatic fields. *Arkiv for Fysik*, *2*(4), 361–365.
- Masters, A. (2015). The dayside reconnection voltage applied to Saturn's magnetosphere. *Geophysical Research Letters*, *42*, 2577–2585. <https://doi.org/10.1002/2015GL063361>
- Masters, A. (2018). A more viscous-like solar wind interaction with all the giant planets. *Geophysical Research Letters*, *45*, 7320–7329. <https://doi.org/10.1029/2018GL078416>
- Masters, A., Eastwood, J. P., Swisdak, M., Thomsen, M. F., Russell, C. T., Sergis, N., et al. (2012). The importance of plasma β conditions for magnetic reconnection at Saturn's magnetopause. *Geophysical Research Letters*, *39*, L08103. <https://doi.org/10.1029/2012GL051372>
- McAndrews, H. J., Owen, C. J., Thomsen, M., Lavraud, B., Coates, A., Dougherty, M., & Young, D. T. (2008). Evidence for reconnection at Saturn's magnetopause. *Journal of Geophysical Research*, *113*, A04210. <https://doi.org/10.1029/2007JA012581>
- Milan, S. E., Lester, M., Cowley, S. W. H., & Brittnacher, M. (2000). Convection and auroral response to a southward turning of the IMF: Polar UVI, CUTLASS, and IMAGE signatures of transient magnetic flux transfer at the magnetopause. *Journal of Geophysical Research*, *105*, 15741–15755. <https://doi.org/10.1029/2000JA900022>
- Palmaerts, B., Radioti, A., Roussos, E., Grodent, D., Gérard, J.-C., Krupp, N., & Mitchell, D. G. (2016). Pulsations of the polar cusp aurora at Saturn. *Journal of Geophysical Research: Space Physics*, *121*, 11952–11963. <https://doi.org/10.1002/2016JA023497>
- Paschmann, G., Papamastorakis, I., Baumjohann, W., Sckopke, N., Carlson, C. W., Sonnerup, B. U. Ö., & Lühr, H. (1986). The magnetopause for large magnetic shear: AMPTE/IRM observations. *Journal of Geophysical Research*, *91*, 11099–11115. <https://doi.org/10.1029/JA091iA10p11099>
- Phan, T.-D., Gosling, J. T., Paschmann, G., Pasma, C., Drake, J. F., Øieroset, M., et al. (2010). The dependence of magnetic reconnection on plasma β and magnetic shear: Evidence from solar wind observations. *The Astrophysical Journal Letters*, *719*, L199–L203. <https://doi.org/10.1088/2041-8205/719/2/L199>
- Quest, K. B., & Coroniti, F. V. (1981). Linear theory of tearing in a high-beta plasma. *Journal of Geophysical Research*, *86*, 3299–3305. <https://doi.org/10.1029/JA086iA05p03299>
- Radioti, A., Grodent, D., Gérard, J.-C., Bonfond, B., Gustin, J., Pryor, W., et al. (2013). Auroral signatures of multiple magnetopause reconnection at Saturn. *Geophysical Research Letters*, *40*, 4498–4502. <https://doi.org/10.1002/grl.50889>
- Raeder, J. (2006). Flux transfer events: 1. Generation mechanism for strong southward IMF. *Annales Geophysicae*, *24*, 381–392. <https://doi.org/10.5194/angeo-24-381-2006>
- Rijnbeek, R. P., Cowley, S. W. H., Southwood, D. J., & Russell, C. T. (1984). A survey of dayside flux transfer events observed by ISEE 1 and 2 magnetometers. *Journal of Geophysical Research*, *89*(A2), 786–800. <https://doi.org/10.1029/JA089iA02p00786>
- Russell, C. T., & Elphic, R. C. (1978). Initial ISEE magnetometer results—Magnetopause observations. *Space Science Reviews*, *22*, 681–715. <https://doi.org/10.1007/BF00212619>
- Russell, C. T., & Elphic, R. C. (1979). ISEE observations of flux transfer events at the dayside magnetopause. *Geophysical Research Letters*, *6*(1), 33–36. <https://doi.org/10.1029/GL006i001p00033>
- Sawyer, R. P., Fuselier, S. A., Mukherjee, J., & Petrincic, S. M. (2019). An investigation of flow shear and diamagnetic drift effects on magnetic reconnection at Saturn's dawnside magnetopause. *Journal of Geophysical Research: Space Physics*, *124*, 8457–8473. <https://doi.org/10.1029/2019JA026696>
- Scurry, L., Russell, C. T., & Gosling, J. T. (1994). Geomagnetic activity and the beta dependence of the dayside reconnection rate. *Journal of Geophysical Research*, *99*(A8), 14811–14814. <https://doi.org/10.1029/94JA00794>
- Slavin, J. A., DiBraccio, G. A., Gershman, D. J., Imber, S. M., Poh, G. K., Raines, J. M., et al. (2014). MESSENGER observations of Mercury's dayside magnetosphere under extreme solar wind conditions. *Journal of Geophysical Research: Space Physics*, *119*, 8087–8116. <https://doi.org/10.1002/2014JA020319>
- Slavin, J. A., Imber, S. M., Boardsen, S. A., DiBraccio, G. A., Sundberg, T., Sarantos, M., et al. (2012). MESSENGER observations of a flux-transfer-event shower at Mercury. *Journal of Geophysical Research*, *117*, A00M06. <https://doi.org/10.1029/2012JA017926>
- Slavin, J. A., Lepping, R. P., Gjerloev, J., Fairfield, D. H., Hesse, M., Owen, C. J., et al. (2003). Geotail observations of magnetic flux ropes in the plasma sheet. *Journal of Geophysical Research*, *108*(A1), 1015. <https://doi.org/10.1029/2002JA009557>
- Smith, A. W., Slavin, J. A., Jackman, C. M., Fear, R. C., Poh, G.-K., DiBraccio, G. A., et al. (2017). Automated force-free flux rope identification. *Journal of Geophysical Research: Space Physics*, *122*, 780–791. <https://doi.org/10.1002/2016JA022994>
- Sonnerup, B. U., & Cahill, L. J. (1967). Magnetopause structure and attitude from explorer 12 observations. *Journal of Geophysical Research*, *72*(1), 171–183. <https://doi.org/10.1029/JZ072i001p00171>
- Sonnerup, B. U. Ö., & Scheible, M. (1998). Minimum and maximum variance analysis. In G. Paschmann, & P. W. Daly (Eds.), *Analysis methods for multi-spacecraft data* (pp. 185–220). Noordwijk: ESA Publication.
- Sun, W. J., Slavin, J. A., Dewey, R. M., Chen, Y., DiBraccio, G. A., Raines, J. M., et al. (2020b). MESSENGER observations of Mercury's nightside magnetosphere under extreme solar wind conditions: Reconnection-generated structures and steady convection. *Journal of Geophysical Research: Space Physics*, *125*, e2019JA027490. <https://doi.org/10.1029/2019JA027490>
- Sun, W. J., Slavin, J. A., Smith, A. W., Dewey, R. M., Poh, G. K., Jia, X., et al. (2020a). Flux transfer event showers at Mercury: Dependence on plasma β and magnetic shear and their contribution to the Dungey cycle. *Geophysical Research Letters*, *47*, e2020GL089784. <https://doi.org/10.1029/2020GL089784>
- Swisdak, M., Opher, M., Drake, J. F., & Aouani Bibi, F. (2010). The vector direction of the interstellar magnetic field outside the heliosphere. *The Astrophysical Journal*, *710*, 1769–1775. <https://doi.org/10.1088/0004-637X/710/2/1769>
- Swisdak, M., Rogers, B. N., Drake, J. F., & Shay, M. A. (2003). Diamagnetic suppression of component magnetic reconnection at the magnetopause. *Journal of Geophysical Research*, *108*, 1218. <https://doi.org/10.1029/2002JA009726>
- Thomsen, M. F., Coates, A. J., Jackman, C. M., Sergis, N., Jia, X., & Hansen, K. C. (2018). Survey of magnetosheath plasma properties at Saturn and inference of upstream flow conditions. *Journal of Geophysical Research: Space Physics*, *123*, 2034–2053. <https://doi.org/10.1002/2018JA025214>
- Thomsen, M. F., Reisenfeld, D. B., Delapp, D. M., Tokar, R. L., Young, D. T., Crary, F. J., et al. (2010). Survey of ion plasma parameters in Saturn's magnetosphere. *Journal of Geophysical Research*, *115*(A10), A10220. <https://doi.org/10.1029/2010JA015267>
- Trattner, K. J., Thresher, S., Trenchi, L., Fuselier, S. A., Petrincic, S. M., Peterson, W. K., & Marcucci, M. F. (2017). On the occurrence of magnetic reconnection equatorward of the cusps at the Earth's magnetopause during northward IMF conditions. *Journal of Geophysical Research: Space Physics*, *122*, 605–617. <https://doi.org/10.1002/2016JA023398>

- Varsani, A., Owen, C. J., Fazakerley, A. N., Forsyth, C., Walsh, A. P., André, M., et al. (2014). Cluster observations of the substructure of a flux transfer event: Analysis of high-time-resolution particle data. *Annales Geophysicae*, 32(9), 1093–1117. <https://doi.org/10.5194/angeo-32-1093-2014>
- Wang, Y. L., Elphic, R. C., Lavraud, B., Taylor, M. G. G. T., Birn, J., Raeder, J., et al. (2005). Initial results of high-latitude magnetopause and low-latitude flank flux transfer events from 3 years of cluster observations. *Journal of Geophysical Research*, 110, A11221. <https://doi.org/10.1029/2005JA011150>
- Xiao, C. J., Pu, Z. Y., Ma, Z. W., Fu, S. Y., Huang, Z. Y., & Zong, Q. G. (2004). Inferring of flux rope orientation with the minimum variance analysis technique. *Journal of Geophysical Research: Space Physics*, 109, A11218. <https://doi.org/10.1029/2004JA010594>
- Young, D. T., Berthelier, J. J., Blanc, M., Burch, J. L., Coates, A. J., Goldstein, R., et al. (2004). Cassini Plasma Spectrometer investigation. *Space Science Reviews*, 114, 1–112. <https://doi.org/10.1007/s11214-004-1406-4>
- Zhang, H., Khurana, K. K., Kivelson, M. G., Angelopoulos, V., Pu, Z. Y., Zong, Q.-G., et al. (2008). Modeling a force-free flux transfer event probed by multiple Time History of Events and Macroscale Interactions during Substorms (THEMIS) spacecraft. *Journal of Geophysical Research*, 113, A00C05. <https://doi.org/10.1029/2008JA013451>
- Zhou, M., Berchem, J., Walker, R. J., el-Alaoui, M., Deng, X., Cazzola, E., et al. (2017). Coalescence of macroscopic flux ropes at the subsolar magnetopause: Magnetospheric Multiscale observations. *Physical Review Letters*, 119(5). <https://doi.org/10.1103/PhysRevLett.119.05510>